Full Title: **Phase-specific premotor inhibition modulates leech rhythmic motor output**

Martina Radice[1,2], Agustín Sanchez Merlinsky[1], Federico Yulita[1,3] and Lidia Szczupak[1,2]

1 Instituto de Fisiología, Biología Molecular y Neurociencias (IFIBYNE-UBA-CONICET), Buenos Aires, Argentina

2 Departamento de Fisiología, Biología Molecular y Celular, Facultad de Ciencias Exactas y Naturales, Universidad de Buenos Aires, Buenos Aires, Argentina

3 Departamento de Física, Facultad de Ciencias Exactas y Naturales, Universidad de Buenos Aires, Buenos Aires, Argentina

Corresponding Author: Lidia Szczupak, lidiaszczupak@gmail.com

ABSTRACT

Understanding how motoneuron activity is finely tuned remains an open question. Leeches are a highly suitable organism for studying motor control due to their well-characterized behaviors and relatively simple nervous system. On solid surfaces leeches display crawling, a rhythmic motor pattern that can be elicited in the isolated nerve cord or even in ganglia isolated from it. This study aimed to learn how this motor output is shaped by concurrent premotor signals. Specifically, we analyzed how electrophysiological manipulation of a premotor nonspiking (NS) neuron, that forms a recurrent inhibitory circuit (homologous to vertebrate Renshaw cells), shapes the leech crawling motor pattern. The study included a quantitative analysis of motor units active throughout the fictive crawling cycle that shows that the rhythmic motor output in isolated ganglia mirrors the phase relationships observed in vivo. Taken together, the study reveals that the premotor NS neurons, under the control of the segmental pattern generator, modulated the degree of excitation of motoneurons during crawling in a phase-specific manner.

INTRODUCTION

Animal locomotion involves the coordination of multiple muscles under the control of the nervous system. Diverse regulatory mechanisms operate at different hierarchical levels within the motor system, narrowing down the degrees of freedom of a system with multiple units, to ensure smooth movements. The overall functional organization of motor systems remains, to a great extent, an open question in both vertebrates and invertebrates (Kiehn, 2016; Arber and Costa, 2018; Barkan and Zornik, 2019; Grätsch et al., 2019), including the mechanisms that operate at the level of the nerve cord (Grillner and El Manira, 2020; McLean and Dougherty, 2015; Gal, 2017; Sengupta and Bagnall, 2023; Calabrese and Marder, 2024). Analysis of this organization across different organisms, developmental stages, and behavioral repertoires has provided fruitful information. Leeches have been highly useful to study motor control due to their robust repertoire of motor behaviors, which are executed by a relatively simple body plan and controlled by a similarly simple nervous system. This system is composed of a chain of 21 midbody ganglia flanked by head and tail brains (Wagenaar, 2015), where each midbody ganglion contains the sensory and motor neurons that innervate the corresponding segment (Muller et al., 1981).

On solid surfaces, leeches exhibit a robust rhythmic motor pattern known as crawling (Figure 1A). This behavior results from waves of elongation and contraction of the body along its antero-posterior axis, as the animal is anchored on the posterior and anterior suckers, respectively (Stern-Tomlinson et al., 1986, Figure 1A). Fictive crawling (*crawling*) can be monitored in the isolated nervous system, where identified interneurons and motoneurons can be recorded intracellularly and extracellularly (Baader, 1997; Baader and Kristan, 1992; Eisenhart et al., 2000). The pattern is characterized by the alternating activation of the motoneurons, such

52 as CV and DE-3, that innervate circular and longitudinal muscles, respectively (Figure 1B). This
53 pattern can be readily evoked by dopamine in the isolated nerve cords (Puhl and Mesce, 2008),
54 in short chains of ganglia (Kearney et al., 2022), and in single isolated ganglia (Puhl and Mesce,
55 2008; Rodriguez et al., 2012). These studies established that each ganglion contains the network
56 responsible for producing the rhythmic motoneuron activity compatible with crawling.

57 Studies on motor behaviors in diverse organisms show that, at the final stage of neural
58 processing, motoneuron activity is controlled by multiple signal sources (El Manira, 2023; Zhen
59 and Samuel, 2015; Rotstein et al., 2017). Analysis of the nature and effects of these signals on
60 the motor pattern is an active field of research. The present work has focused on the role played
61 by nonspiking (NS) premotor neurons on leech crawling. These neurons are present as bilateral
62 pairs in each segmental ganglion and are functional homologs of the Renshaw cells (Szczupak,
63 2014). Each pair of NS neurons is at the center of a recurrent inhibitory circuit mediated by
64 chemical and electrical synaptic connections with the motoneurons (Figure 1C) (Rela and
65 Szczupak, 2003; Rodriguez et al., 2009). In the context of this circuit the activity of excitatory
66 motoneurons evokes chemically mediated inhibitory synaptic potentials in NS. Additionally, the
67 NS neurons are electrically coupled to virtually all excitatory motoneurons via rectifying
68 junctions that conduct when the transjunction NS-motoneuron potential is negative. In
69 physiological conditions this coupling favors the transmission of inhibitory signals from NS to
70 motoneurons. Given this recurrent inhibitory circuit, NS premotor neurons can operate as
71 modulators of motoneuron activity. This study aimed to evaluate the role of the known
72 connectivity of the premotor NS neuron (Figure 1C) in shaping the crawling motor pattern. The
73 experimental results reveal that NS mediates a reduction of the firing frequency of motoneurons
74 recruited during a specific phase of crawling.

75 **RESULTS**

76 **NS membrane potential oscillations during *crawling***

77 To study the role that premotor NS neurons play in fictive crawling (*crawling)*, we first analyzed
78 the correspondence between NS electrophysiological activity and the motoneuron output during
79 this motor pattern. Since motoneuron DE-3 (dorsal excitor 3), which innervates the longitudinal
80 dorsal muscle fibers, is the most robust proxy of *crawling* (Puhl and Mesce, 2008), extracellular
81 recordings of this motoneuron in the DP nerve were combined with NS intracellular recordings.
82 The NS membrane potential showed rhythmic oscillations tuned to DE-3 activity, with
83 hyperpolarizations occurring in conjunction with DE-3 bursts and depolarizations during DE-3
84 silent phases (Figure 2A). A cross-correlation analysis between NS and DE-3 revealed a marked
85 anticorrelation, with a cross-correlation index of -0.61 ± 0.03 (mean ± SEM) at a lag close to 0
86 sec (0.24 ± 0.10 s) (Figure 2B). This result indicates that NS hyperpolarization takes place in
87 phase with DE-3 bursts.

88 In the frame of the recurrent inhibitory circuit, NS is the target of inhibitory signals
89 evoked by excitatory motoneurons via chemically-mediated polysynaptic pathways (Rela and
90 Szczupak, 2003, Figure 1C). Thus, it could be hypothesized that the NS hyperpolarizations
91 observed during *crawling* resulted from inputs originating in DE-3 and other motoneurons that
92 fire in phase with it. If this hypothesis was correct, the onset of DE-3 bursts should precede the
93 onset of NS hyperpolarization. Because the cross-correlation was performed on binned DE-3
94 firing frequency curves, the peak lag reported does not offer a proper estimation of the relative
95 timing between the two signals. To gain a more precise assessment, NS intracellular recordings
96 were segmented into individual cycles and aligned with the first spike of the corresponding DE-3
97 burst (Figure 2C). As shown in the figure, because of the NS membrane potential oscillations it

98 is not possible to establish a sharp onset for the NS hyperpolarizing response. However, the
99 example illustrates that the onset of the DE-3 bursts occurred after NS hyperpolarization was
100 already initiated. These findings rule out the possibility that the NS hyperpolarization was
101 originated by DE-3 bursting. Instead, they suggest that NS and DE-3 receive concomitant
102 rhythmic inputs of opposite sign—that is, hyperpolarizing inputs in NS and depolarizing ones in
103 DE-3.

104 To further analyze the putative concomitant inputs from the pattern generator onto NS
105 and DE-3, we evaluated the correlation between different features of their rhythmic activity
106 (Figure 2A). We found no relationship between the amplitude of NS hyperpolarization and DE-3
107 mean firing frequency. However, surprisingly, the former exhibited a high correlation with DE-3
108 burst duration (Figures 2D-E). This result led to examining how the amplitude of NS
109 hyperpolarization related to the time between consecutive DE-3 bursts (interbursts time),
110 preceding (pre) and following (post) the NS hyperpolarization (Figure 2A). The data show a
111 significant correlation of the amplitude of NS hyperpolarization with the pre-interburst duration,
112 but not with the post-interburst duration (Figure 2F-G). Taken in consideration the putative
113 model presented in Figure 1C, in which the oscillator units C and E inhibit each other, the longer
114 the activity of unit E, the larger the rebound in unit C and its downstream effects on NS
115 hyperpolarization and on DE-3 burst duration.

116 These results indicate that, in addition to the known recurrent inhibitory circuit between
117 NS and motoneurons, NS neurons receive an inhibitory signal during *crawling*, which is in phase
118 with DE-3 activity. This inhibitory signal seems to have originated from the same source that
119 activates DE-3 motoneurons. In that case, it seems puzzling to find a lack of correlation between
120 NS hyperpolarization amplitude and DE-3 firing frequency. However, this observation might be

121 explained by considering that DE-3 is subjected to two counteracting effects at the same phase:
122 an excitatory input from the oscillator unit C and an inhibitory input from NS via the rectifying
123 electrical junctions (Figure 1C).
124
125 **Effect of NS on DE-3 activity during *crawling***
126 To test whether the inhibitory signal in NS is transmitted to the motoneurons, the premotor
127 neuron was transiently removed from the circuit. In line with the properties of the rectifying
128 electrical synapse between NS and the motoneurons, depolarizing NS neurons is equivalent to
129 disconnecting them from the network (Rela and Szczupak, 2007).
130 Depolarizing steps applied in NS neurons in the course of *crawling* episodes (Figure 3A)
131 shifted their membrane potential beyond +100 mV, well above the average membrane potential
132 of the motoneurons. To account for potential drifts in *crawling* features over time, we compared
133 two series of experiments: one in which NS was subjected to depolarizing steps (depo) and a
134 control (ctrl) in which it was not. We assessed changes in cycle period, DE-3 mean firing
135 frequency (mFF), burst duration and duty cycle for both treatments (depo, ctrl) across different
136 epochs (pre, test, post).
137 Transient NS depolarizations had no effect on the *crawling* period (measured in end-to-
138 end cycles, see Materials and Methods), DE-3 burst duration and duty cycle (Figure 3B), but
139 produced a 60% increase in DE-3 mFF (Figure 3B-C).
140 In the control series the analysis of *crawling* features over time shows that cycle period
141 and DE-3 burst duration decreased over epochs, while the duty cycle remained constant. Similar
142 results were obtained when cycles were segmented from start-to-start (data not shown). Thus,

143 throughout the dopamine perfusion the motor pattern exhibited an acceleration but the duty cycle
144 remained stable.
145 This series of experiments proves that, as predicted from the known circuit (Figure 1C),
146 inhibitory signals onto NS premotor neurons counteracted the excitatory drive onto DE-3
147 motoneurons during *crawling*, limiting its firing frequency.
148
149 **A more comprehensive view of *crawling***
150 As indicated above, the activity of motoneuron DE-3 has been widely used as a proxy of
151 *crawling*. However, focusing on a single motoneuron neglects possible effects of NS on other
152 phases of the motor pattern. To evaluate whether the effect of the premotor NS neuron extends to
153 other motoneurons active during *crawling*, we performed extracellular recordings of DP, AA and
154 PP root nerves. Single units were identified using a spike sorting algorithm (Figure 4Ai-Aii) that
155 enabled a systematic analysis of their activity. The firing pattern of detected units (Figure 4Aiii)
156 was expressed as binned firing frequency (bFF). Because DE-3 is used as a reference marker of
157 the cycle, segmentation of the traces was performed using the start-to-start approach (see
158 Material and Methods). This rhythmic activity shows that some units fire during the contraction
159 phase, defined by DE-3 activity, while others fire during the elongation phase.
160 Plotting the bFF of the different rhythmic units as a function of phase within a *crawling*
161 cycle (start-to-start) allowed for the manual classification of the unit. Based on their activity
162 profile relative to DE-3 three types were identified: In-Phase, Anti-Phase, or In-Phase-Early-
163 Onset (Figure 4B). The In-phase units fire simultaneously with DE-3, the Anti-Phase units fire in
164 between DE-3 bursts, and the In-Phase-Early-Onset are active in phase with DE-3 but start firing
165 before DE-3 burst onset (Figure 4C).

While multiple extracellular recordings have been performed previously (Eisenhart et al., 2000), these results present the first quantitative analysis of motor units activated throughout the *crawling* cycle. The In-Phase units are expected to control the contraction stage by exciting or inhibiting the longitudinal or circular muscles, respectively, and the Anti-Phase units to control the elongation stage by exciting or inhibiting the circular or longitudinal muscles, respectively. It is plausible that In-Phase-Early-Onset are inhibitors of circular muscles, preparing the conditions for a fast contraction phase. Further studies should confirm this hypothesis.

Comparison of the motor pattern in single ganglia and in intact animals

The assumption that the above description of the crawling motor pattern *ex vivo*, in isolated single ganglia, represents the neural correlate of the actual behavior requires qualitative and quantitative validation. To this end intact leeches were monitored during crawling. The analysis was performed by tracking nine dots painted along the dorsal longitudinal midline of the leech, which divided the body into 8 sections (Figure 5A). Because ganglia are located in highly conserved positions relative to the length of the animal (Figure 5B, Kearney et al. 2022), the relative distance from the head can be used to infer which ganglia are included within the 8 sections mentioned above. We focused the analysis on sections delimited by points 4-5 and 5-6, that correspond to the range of segmental ganglia included in the *ex vivo* studies (ganglia 8 to 15) (Figure 5A-B). For electrophysiological data the frame of analysis was the cycle of DE-3 rhythmic activity and, equivalently, for the behavioral data the frame of analysis was the crawling step (see Materials and Methods).

Figure 5C shows a representative trace of a series of whole length waves, that were divided into discrete steps (see Materials and Methods), and the corresponding measurements in

189 the section delimited by the dots 4 and 5. Within each crawling step, four stages were identified
190 in the studied sections (Figure 5C): the elongation stage (marked by an increase in section
191 length), the contraction stage (marked by a decrease in section length) and two isometric stages
192 flanking the dynamic stages. The plot in Figure 5D shows the section length of different steps by
193 the same animal, normalized by the step duration, and illustrates the variability of the step
194 dynamics.

195 For a quantitative comparison of the *in vivo* and *ex vivo* experiments the following
196 variables were evaluated: period of the rhythmic pattern and duty cycle of the different phases.
197 While the average cycle period (end-to-end) recorded in isolated ganglia was of 15.22 ± 3.21 s (n
198 = 6), the average duration of the leech step was of 7.49 ± 0.50 s (n=6). The latter value is similar
199 to that reported in previous studies (Stern-Tomlinson et al., 1986; Baader and Kristan, 1992).
200 Thus, in the intact animal the rhythmic activity was twice as fast as in the isolated ganglion,
201 suggesting that peripheral signals may accelerate the rhythmic behavior, as already described in
202 other animals (Pulver et al., 2015; Fushiki et al., 2016). However we cannot rule out that
203 activation of the rhythmogenic circuit in isolated ganglia may fail to activate a circuit component
204 responsible for speeding the rhythm.

205 It seems natural to correlate the activity of the Anti-Phase and In-Phase of e*x vivo* studies
206 with the elongation and contraction stages of *in vivo* behavior. But the isometric stages displayed
207 *in vivo* have no obvious counterpart in the electrophysiological recordings. It is important to
208 consider that the rhythmic movement of successive segments along the antero-posterior axis of
209 the animal requires a delay signal that allows the appropriate propagation of the metachronal
210 wave, and this signal is probably absent in the isolated ganglion. In consequence, for the
211 comparison of the duty cycle, the *in vivo* isometric stages were ignored, and only the duration of

212 the dynamic fraction of the step was taken in consideration. In turn, the behavioral duty cycle
213 was calculated as the ratio between the elongation or contraction stage duration over the dynamic
214 step duration. Thus measured, the duty cycle of the elongation stage was 0.65 ± 0.01 and that of
215 the contraction was 0.35 ± 0.01 (Figure 5E). These values are noticeably close to the duty cycle
216 of the Anti-Phase units (0.64 ± 0.07) and of the DE-3 motoneurons (0.32 ± 0.03) (Figure 5E)
217 measured in the isolated ganglia.
218 These results show that the dynamic pattern described by motoneurons recorded in
219 isolated ganglia reflects the phase relation observed in the corresponding body section *in vivo*.
220
221 **Effect of NS on the activity of the different types of motoneurons during *crawling***
222 The results shown in Figure 5 support the view that the activity recorded in single ganglia
223 reflects the neuronal control of the rhythmic pattern underlying crawling. Based on this premise
224 the recording of multiple units presented above was used to evaluate the influence of NS on units
225 active at different *crawling* stages (Figure 6Ai-ii). Does NS depolarization affect the activity of
226 other units In-Phase with DE-3? How are Anti-Phase units affected by this experimental
227 maneuver? The activity of the motoneurons was characterized using two metrics: maximum bFF
228 (Max bFF) to assess activity level, and relative half width (Rel HW) to evaluate the duty cycle.
229 To enable a comparison with the other units, the data for DE-3 was reanalyzed in this manner.
230 NS depolarization produced an increase in DE-3 Max bFF of around 60% (as shown
231 above), while this variable remained stable throughout control experiments (Figure 6B).
232 Different from DE-3, In-Phase units showed a marked decrease in the maximal bFF along time
233 in control conditions, but similar to DE-3, this variable underwent an increase of around 50%

upon NS depolarization (Figure 6B). Given the temporal drop detected in the control series this increase is probably an underestimation of the NS effect on the In-Phase firing frequency.

The Anti-Phase units also showed a marked drop in the maximum bFF along time in control conditions but in this case the effect of NS depolarization was limited to counteracting this decrease (Figure 6B). NS depolarization did not affect the maximum bFF of the In-Phase-Early-Onset units (Figure 6B).

Regarding the relative HW, the effect of NS depolarization was limited to preventing the decrease of this variable over time only for In-Phase units. It is possible that by increasing the firing frequency of the In-Phase units, the NS depolarization kept the firing span of these units at a more stable level (Figure 6C).

The statistical analyses performed for these results are detailed in Supplementary Table 2.

In summary, the rhythmic NS hyperpolarizations selectively limited the activity of motoneurons that are active in phase with its inhibitory inputs, specifically those controlling the contraction phase. This selective effect highlights the role of NS in modulating specific phases of the motor pattern without disrupting the overall coordination of elongation and contraction phases. It is worth noting that the fact that the firing frequency of Anti-Phase MNs was not affected by NS depolarization indicates that this experimental manipulation did not cause a generalized change in the activity of MNs but achieved the desired goal of temporarily removing the rhythmic NS hyperpolarization. On the other hand, the fact that In-Phase-Early-Onset activity was also unaffected by NS depolarization confirms that these motoneurons constitute a distinct group from the In-Phase units. Furthermore, this suggests that these units might be inhibitory motoneurons that are not connected to the NS via the recurrent inhibitory circuit (Rela and Szczupak, 2003; Wadepuhl, 1989).

258 **DISCUSSION**

259 The present study shows that phase specific inhibitory signals, delivered by the functional
260 homolog of Renshaw cells in the leech (Szczupak, 2014), modulate the degree of excitation of
261 the motoneurons responsible for the contraction phase of *crawling*. This effect was phase
262 specific, as motoneurons active in the rest of the cycle were not affected. NS is a premotor
263 neuron that operates at the center of a recurrent inhibitory circuit (Rela and Szczupak, 2003;
264 Rodriguez et al., 2009) and thus the initial hypothesis suggested that the effect on *crawling* was
265 mediated entirely by this circuit. However, the results show that the inhibitory signal did not
266 originate at the level of the motoneurons themselves but, most probably, at the crawling
267 oscillator. The marked temporal correlation between the neurons active during the contraction
268 phase and NS hyperpolarizations suggests that the excitatory signals onto the motoneurons and
269 the hyperpolarizing signals onto NS were driven by the same upstream element (e.g. the element
270 in the oscillator that controls the contraction phase). This result further feeds the homology
271 between vertebrate Renshaw cells and leech NS neurons in that the formers are not only targeted
272 by motoneuron inputs but by rhythmogenic premotor elements as well (Nishimaru et al., 2006).
273 Nonetheless, the results do not rule out that the existing recurrent inhibitory circuit contributes to
274 the hyperpolarization of NS.

275 In summary, we propose that the crawling oscillator releases a dual signal onto the
276 motoneurons that control the contraction phase: a direct excitatory input that elicits the rhythmic
277 bursts and a concurrent inhibitory input via NS (Figure 7). Coherent with this interpretation, the
278 activity level of the Anti-Phase units was not influenced by these inhibitory signals.

279 The corroboration of a dual counteracting set of actions on motoneuron output calls for a
280 functional interpretation. In a characterization of the electrophysiological properties of leech

281 motoneurons it was shown that DE-3 can reach a firing frequency that exceeds 100 Hz (Perez-
282 Etchegoyen et al., 2011) while the maximal muscle tension that this motoneuron can evoke is
283 achieved at around 25 Hz (Mason and Kristan, 1982). Additionally, it is relevant to consider that
284 the population of motoneurons that activate longitudinal muscles is linked by ohmic coupling
285 that can result in mutual excitation (Fan et al., 2005; Ort et al., 1974, Ashaber et al., 2021). As a
286 result, when all the activators of longitudinal muscles are excited during the contraction phase,
287 the excitatory spread can lead to runaway motoneuron activity (Hennequin et al., 2017). An
288 inhibitory signal imposed on NS can spread to all the motoneurons simultaneously (Rela and
289 Szczupak, 2003; Rodriguez et al., 2009; Wadepuhl, 1989) and thus limit the activity of the whole
290 motoneuron population.

291 Previous work showed that leech motoneurons are subjected to a generalized inhibition
292 mediated by GABA (Baca et al., 2008) while the electrically mediated inhibition exerted by NS
293 shown here is phase-specific. The existence of concurrent excitation and inhibition has been
294 revealed in vertebrate motor networks, where it was proposed as a balancing factor (Kishore et
295 al., 2014; Parkis et al., 1999; Petersen et al., 2014). In line with the present results, experiments
296 performed in zebrafish showed that in-phase inhibition originates from a set of premotor neurons
297 that comprise the Renshaw cells (Callahan et al., 2019). Neurophysiological studies in the leech
298 offer the particular advantage of allowing electrical manipulation of individual neurons in wild-
299 type adults, where they can be readily recognized by their anatomical and electrophysiological
300 characteristics. In this sense the present study offers clear-cut evidence of the dual signal
301 motoneurons receive in the course of motor control from an identified premotor element.

302 The results further highlight the notion that knowing the connectivity among neurons is
303 not sufficient to deduce its functional operation, as the dynamical interplay among them is highly
304 relevant to understand its physiological role.
305
306 **Structure of *crawling* based on MN activity and behavior**
307 Evaluation of phase specificity required a more comprehensive tracking of motoneuron activity
308 throughout the cycle and we addressed this demand through the analysis of the activity of
309 multiple motoneurons. In the present study we show that in the course of *crawling* DE-3 neurons
310 fire concurrently with neurons that reach the periphery mainly through the PP and the AA roots.
311 Based on the classical description of Ort and collaborators (1974) the spikes in phase with DE-3
312 recorded in the PP root are likely to correspond to VE-4 (ventral-excitor 4), DE-5, DE-7 and VE-
313 8, while those recorded in AA are likely to correspond to DE-107 and VE-108.
314 To learn how the motoneuron readout compares with the rhythmic body movements that
315 take place in crawling we presented behavioral studies that focused on the sections of the leech
316 body that match the range of ganglia used in the electrophysiological studies. The comparison
317 shows two main differences. The period of the rhythmic animal behavior was half that measured
318 in the fictive behavior at the isolated ganglia. In addition, at the behavioral level the actual
319 elongation-contraction gestures were flanked by isometric stages, while in dopamine-induced
320 *crawling* studied in isolated ganglia the rhythmic activity of the motoneurons appears as the
321 alternation between units In-Phase with DE-3 and Anti-Phase of DE-3, with no clear references
322 for isometric phases. The absence of descending brain signals and/or peripheral signals are
323 assumed as important factors in determining the cycle period and the sequence at which the
324 different behavioral stages take place. However, it is noteworthy that taking the isometric stages

aside, the sequence of events, and the proportion of the active cycle dedicated to elongation and contraction were remarkably similar in both experimental settings. This suggests that the network activated in the isolated ganglion is the one underlying the motor behavior.

329 **MATERIALS AND METHODS**

330 **Biological Preparation**

331 Leeches (*Hirudo* sp.), weighing 1–3 g, were sourced from commercial suppliers (Niagara
332 Leeches, Cheyenne, WY, United States and Biopharm, UK) and kept at 20°C in artificial pond
333 water. These animals are hermaphrodites.

334 Studies were conducted in isolated single ganglia obtained from segments 8th to 13th.
335 The ganglia were dissected with one dorsal posterior (DP), posterior (PP) and anterior (AA)
336 nerve roots attached. The tissue was bathed in normal saline (in mM: 115 NaCl, 4 KCl, 1.8
337 $CaCl_2$, 1 $MgSO_4$, 10 Hepes, 10 glucose; pH 7.4) at room temperature (20–25°C) and pinned to
338 Sylgard (Dow Corning) in a recording chamber. The sheath covering the ganglion was dissected
339 away, exposing the neuronal cell bodies to the external solution.

340

341 **Electrophysiological Recordings**

342 Intracellular somatic recordings were conducted using microelectrodes pulled from borosilicate
343 capillary tubing (A-M Systems, Inc., Carlsborg, WA, United States), filled with 3 M potassium
344 acetate (resistance 20–40 MΩ). The electrodes were connected to an Axoclamp 2B amplifier
345 (Axon Instruments; Union City, CA, United States) operating in bridge mode. Extracellular
346 activity from DP, PP, and AA nerves was recorded using suction electrodes connected to a
347 differential a.c. amplifier (Neuroprobe 1700, A-M Systems, Inc., Carlsborg, WA, United States).
348 Intra- and extracellular recordings were digitized through an analog-digital converter (Digidata
349 1440, Axon Instruments, Union City, CA, United States) and acquired with Clampex 9.2 (Axon
350 Instruments, Union City, CA, United States) at a sampling rate of 20 kHz. Premotor NS neurons
351 were identified by their soma location and electrophysiological properties (Rela et al., 2009).

352 To induce fictive crawling (*crawling*), ganglia were superfused with 75 μM dopamine
353 hydrochloride (Sigma-Aldrich, St. Louis, MO, United States), freshly prepared at the beginning
354 of each experimental day (Puhl and Mesce, 2008). Only one episode was evoked per ganglion.
355 The rhythmic motor pattern was monitored via extracellular recording of the DP nerve, where
356 the largest spike corresponds to the DE-3 motoneuron, one of the motoneurons innervating the
357 longitudinal muscles (Ort et al., 1974).
358 When testing the effect of NS neurons, depolarizing pulses of +5 nA to +7 nA were
359 injected into its soma through the intracellular electrode. Between four and five *crawling* cycles
360 before and after a depolarizing pulse were left unaffected to obtain control pre and post rhythmic
361 epochs.
362
363 **Behavioral Experiments**
364 Leeches were anesthetized by placing individuals at −20◦C for 5 to 10 minutes. Then the skin of
365 the animal was dried, and nine points of water-based paint were applied along its dorsal
366 longitudinal midline (Figure 5A). When the animals recovered they were allowed to crawl onto a
367 graph paper sheet covered with a transparent plastic surface. Crawling was filmed at 60 fps with
368 a digital camera (Sony ILCE-A6400) supported above the arena. The position of each point
369 painted on the leech skin was tracked using DeepLabCut version 2.3.5 (He et al., 2016;
370 Insafutdinov et al., 2016; Mathis et al., 2018; Nath et al., 2019). To this end, 338 frames
371 randomly selected from 66 videos of 8 leeches were used for manually labeling the painted dots,
372 and used for training a ResNet_50-based neural network for automating the detection.
373 To characterize crawling, steps were defined by the frames in which the algorithmic sum
374 of the following values was at a minimum: 1) the whole length of the leech, 2) the velocity of the

375 most anterior dot, and 3) the velocity of the most posterior dot (Figure 5C). Steps where
376 DeepLabCut failed to detect any of the nine points on the animal were discarded. After dividing
377 the animal displacement into steps, we performed a quantitative analysis of the changes in the
378 length of the animal sections (defined between each pair of points) over time. Specifically, the
379 sections delimited by the painted points 4-5 and 5-6 were chosen since they include the range of
380 ganglia considered in the electrophysiological studies (8-15). The length traces of each leech
381 were filtered using a Gaussian filter (sigma of 0.25 s). For each step, the duration of the
382 elongation and contraction phases within a section was calculated by using the maximum length
383 as the boundary between these phases. The onset of elongation and the end of contraction were
384 determined by detecting knee points, as described by Satopaa et al. (2011, Figure 5C).
385
386 **Spike Sorting**
387 Extracellular recordings were spike sorted using a custom-written algorithm which relies on a
388 template matching-based method based on (Pouzat et al., 2002), incorporating a t-SNE model
389 (Pedregosa et al., 2011; Van der Maaten and Hinton, 2008). Because spike sorting is sensitive to
390 misclassification, the resulting output was manually curated to address whether a single cluster
391 of waveforms was self-consistent with a single neuron (Hill et al., 2011). During manual
392 curation, all clusters of putative spike events were evaluated. Clusters containing two well
393 defined groups of waveforms were split and pairs of clusters with similar waveforms and
394 temporally coordinated activity were merged. Clusters that had inconsistent waveforms and
395 could not be split into clusters with well-defined waveforms were discarded. After this
396 procedure, each cluster was considered a single motor unit.

397 To select for rhythmic units, autocorrelations were performed considering the first four
398 cycles of the fictive behavior. Units whose autocorrelogram included at least 2 peaks with a
399 correlation coefficient greater than 0.25 were considered rhythmic.
400
401 **Data Processing**
402 DE-3 spike times were derived from DP nerve recordings using the spike sorting algorithm
403 mentioned above. DE-3 bursts were considered as such if they comprised at least 10 spikes with
404 a mean firing frequency of 8 Hz, where the separation between two subsequent spikes occurred
405 with a maximum separation of 0.5 seconds. Burst duration was calculated as the time difference
406 between the last and first DE-3 spikes in each burst. Cycle period was calculated in two different
407 ways: as the time difference between the last (end-to-end), or the first spikes (start-to-start) of
408 subsequent DE-3 bursts, and is reported accordingly. Duty cycle was calculated as the ratio
409 between burst duration and period. The mean firing frequency (mFF) of each burst was
410 calculated as the number of spikes over the burst duration. The binned firing frequency (bFF) of
411 DE-3, or any other unit, was obtained by binning the number of spikes along the recording using
412 a 0.05 s or a 0.5 s interval, for Figure 2 and Figure 6, respectively. For cross-correlation analysis,
413 the DE-3 bFF was filtered using a Gaussian filter (sigma of 150 ms).
414 For the cross-correlation between NS membrane potential and DE-3 firing frequency, the
415 intracellular recording of NS was resampled to match the data rate of DE-3 bFF. To determine
416 the amplitude of NS hyperpolarization, a baseline membrane potential was established using a
417 Gaussian filter (sigma of 5 s) applied to the entire trace. The amplitude was calculated as the
418 difference between the baseline value at the start of the DE-3 burst and the minimum membrane
419 potential reached by NS during the corresponding burst (see Figure 2A).

When NS depolarization was implemented, the cycles including the onset or offset of the current pulse were excluded, and the traces were divided into three epochs: pre, test, and post. Control experiments were treated similarly.

When analyzing the activity of the units obtained by spike sorting, the maximum bFF value and relative half width were obtained from curves displaying bFF versus cycle-phase (time normalized to the period of each cycle). The relative half width was calculated as the width at half the maximum bFF value.

Data processing was performed using custom written Python scripts.

Statistical Analysis

All statistical analyses were performed using R (R Core Team, 2020). For every analysis, the structure of random factors was kept maximal whenever possible. The specific random factors considered in each case are detailed in Supplementary Tables 1 and 2.

To analyze the correlation between the amplitude of NS hyperpolarization and different *crawling* features (Figure 2D-G), the lmer function from the lmerTest package (Kuznetsova et al., 2017) was used to perform linear mixed models (LMM) with the experiment as a random factor.

To analyze the effect of NS depolarization on motoneuron activity, the data was analyzed using mixed-effects models with two fixed factors: epoch (pre, test, post) and treatment (control, depolarization). All models included motor units as a random factor. Each ganglion was also included as a random factor. The effect of NS depolarization was analyzed with the glmmTMB function from the glmmTMB package (Brooks et al., 2017) to perform a generalized linear mixed model (GLMM) or with the lmer function to perform a LMM. For the GLMM, we used a

student-t distribution (t_family) with the identity link or Gamma family with a log link as indicated in Supplementary Tables 1 and 2. The significance of a factor was determined with a likelihood-ratio test for the GLMM or an F-test for the LMM. This was done by comparing the model including the factor with a model dropping that factor. Pairwise simple contrasts were performed within the treatment factor and between the epoch factor using the *emmeans* package and the Tukey correction were applied to obtain the p values.

To analyze a possible temporal drift on *crawling* features we considered the data of control experiments and used mixed-effects models with epoch (pre, test, post) as a fixed factor and units as a random factor. Supplementary Tables 1 and 2 specifies the models used for each analysis.

Acknowledgments: The authors thank Drs. Violeta Medan, Graciela Kearney, Alejandro Cámera and Ronald Calabrese for highly valuable comments on the manuscript. This work was supported by the following grants to LS: PICT 2016–2073 from Agencia Nacional de Promoción Científica y Tecnológica; UBACyT 20020150100179BA from Universidad of Buenos Aires and Human Frontier Science Program (RGP0060/2019).

460 **REFERENCES**

461

462 Arber, S., and R.M. Costa. 2018. Connecting neuronal circuits for movement. *Science*.
463 360:1403-1404.
464 Ashaber, M., Tomina, Y., Kassraian, P., Bushong, E. A., Kristan, W. B., Ellisman, M. H., &
465 Wagenaar, D. A. (2021). Anatomy and activity patterns in a multifunctional motor neuron and its
466 surrounding circuits. *eLife*, *10*, e61881. https://doi.org/10.7554/eLife.61881
467 Baader, A.P. 1997. Interneuronal and motor patterns during crawling behavior of semi-intact
468 leeches. *J Exp Biol.* 200:1369-1381.
469 Baader, A.P., and W.B. Kristan. 1992. Monitoring neuronal activity during discrete behaviors: a
470 crawling, swimming and shortening device for tethered leeches. *J. Neurosc. Meth.* 43:215-223.
471 Baca, S.M., A. Marín-Burgin, D.A. Wagenaar, and W.B. Kristan. 2008. Widespread inhibition
472 proportional to excitation controls the gain of a leech behavioral circuit. *Neuron*. 57:276-289.
473 Barkan, C. L., & Zornik, E. (2019). Feedback to the future: motor neuron contributions to central
474 pattern generator function. *The Journal of experimental biology*, 222(Pt 16), jeb193318.
475 https://doi.org/10.1242/jeb.193318
476 Brooks, M.E., K. Kristensen, K.J. Van Benthem, A. Magnusson, C.W. Berg, A. Nielsen, H.J.
477 Skaug, M. Machler, and B.M. Bolker. 2017. glmmTMB balances speed and flexibility among
478 packages for zero-inflated generalized linear mixed modeling. *The R journal*. 9:378-400.
479 Calabrese RL & Marder E. (2024). Degenerate Neuronal and Circuit Mechanisms Important for
480 Generating Rhythmic Motor Patterns. *Physiological Reviews*.
481 Callahan, R.A., R. Roberts, M. Sengupta, Y. Kimura, S.-i. Higashijima, and M.W. Bagnall.
482 2019. Spinal V2b neurons reveal a role for ipsilateral inhibition in speed control. *Elife*. 8:e47837.
483 Eisenhart, F.J., T.W. Cacciatore, and W.B. Kristan. 2000. A central pattern generator underlies
484 crawling in the medicinal leech. *J Comp Physiol A*. 186:631-643.
485 El Manira, A. 2023. Modular circuit organization for speed control of locomotor movements.
486 *Current Opinion in Neurobiology*. 82:102760.
487 Fan, R.J., A. Marín-Burgin, K.A. French, and W.O. Friesen. 2005. A dye mixture (Neurobiotin
488 and Alexa 488) reveals extensive dye-coupling among neurons in leeches; physiology confirms
489 the connections. *J Comp Physiol A*. 191:1157-1171.

Fushiki, A., Zwart, M. F., Kohsaka, H., Fetter, R. D., Cardona, A., and Nose, A. (2016). A circuit mechanism for the propagation of waves of muscle contraction in *Drosophila*. *eLife* 5:e13253.

Gal, J.-P.L., Dubuc, R. and Smarandache-Wellmann, C. 2017. Coordination of Rhythmic Movements. *In* Neurobiology of Motor Control. S.L.H.a.A. Büschges, editor. Wiley Blackwell. 305-332.

Grätsch, S., Büschges, A., & Dubuc, R. (2019). Descending control of locomotor circuits. *Current Opinion in Physiology*.

Grillner, S., and A. El Manira. 2020. Current Principles of Motor Control, with Special Reference to Vertebrate Locomotion. *Physiological Reviews*. 100:271-320.

He, K., X. Zhang, S. Ren, and J. Sun. 2016. Deep residual learning for image recognition. *In* Proceedings of the IEEE conference on computer vision and pattern recognition. 770-778.

Hennequin, G., Agnes, E. J., & Vogels, T. P. (2017). Inhibitory Plasticity: Balance, Control, and Codependence. *Annual review of neuroscience*, *40*, 557–579.

Hill, D. N., Mehta, S. B., and Kleinfeld, D. (2011). Quality metrics to accompany spike sorting of extracellular signals. *J. Neurosci*. 31, 8699–8705.

Insafutdinov, E., L. Pishchulin, B. Andres, M. Andriluka, and B. Schiele. 2016. Deepercut: A deeper, stronger, and faster multi-person pose estimation model. *In* Computer Vision–ECCV 2016: 14th European Conference, Amsterdam, The Netherlands, October 11-14, 2016, Proceedings, Part VI 14. Springer. 34-50.

Kearney, G., M. Radice, A. Sanchez Merlinsky, and L. Szczupak. 2022. Intersegmental Interactions Give Rise to a Global Network. *Front Neural Circuits*. 16.

Kiehn, O. 2016. Decoding the organization of spinal circuits that control locomotion. *Nat Rev Neurosci*. 17:224-238.

Kishore, S., M.W. Bagnall, and D.L. McLean. 2014. Systematic shifts in the balance of excitation and inhibition coordinate the activity of axial motor pools at different speeds of locomotion. *Journal of Neuroscience*. 34:14046-14054.

Kuznetsova, A., P.B. Brockhoff, and R.H.B. Christensen. 2017. lmerTest package: tests in linear mixed effects models. *Journal of statistical software*. 82.

Marín-Burgin, A., and L. Szczupak. 2003. Network interactions among sensory neurons. *J. Comp. Physiol. A*. 189:59-67.

Mason, A., and W.B. Kristan. 1982. Neuronal excitation, inhibition and modulation of leech longitudinal muscle. *J. Comp. Physiol.* 146:527-536.

Mathis, A., P. Mamidanna, K.M. Cury, T. Abe, V.N. Murthy, M.W. Mathis, and M. Bethge. 2018. DeepLabCut: markerless pose estimation of user-defined body parts with deep learning. *Nature neuroscience*. 21:1281-1289.

McLean, D.L., and K.J. Dougherty. 2015. Peeling back the layers of locomotor control in the spinal cord. *Curr Opin Neurobiol*. 33:63-70.

Muller, K.J., J.G. Nicholls, and G.S. Stent. 1981. Neurobiology of the leech. Cold Spring Harbor Laboratory, Cold Spring Harbor, NY.

Nath, T., A. Mathis, A.C. Chen, A. Patel, M. Bethge, and M.W. Mathis. 2019. Using DeepLabCut for 3D markerless pose estimation across species and behaviors. *Nature protocols*. 14:2152-2176.

Nishimaru, H., C.E. Restrepo, and O. Kiehn. 2006. Activity of Renshaw cells during locomotor-like rhythmic activity in the isolated spinal cord of neonatal mice. *J Neurosci*. 26:5320-5328.

Ort, C.A., W.B. Kristan, and G.S. Stent. 1974. Neuronal control of swimming in the medicinal leech. *J Comp Physiol A*. 94:121-154.

Parkis, M., X.-W. Dong, J. Feldman, and G. Funk. 1999. Concurrent inhibition and excitation of phrenic motoneurons during inspiration: phase-specific control of excitability. *Journal of Neuroscience*. 19:2368-2380.

Pedregosa, F., G. Varoquaux, A. Gramfort, V. Michel, B. Thirion, O. Grisel, M. Blondel, P. Prettenhofer, R. Weiss, and V. Dubourg. 2011. Scikit-learn: Machine learning in Python. *the Journal of machine Learning research*. 12:2825-2830.

Perez-Etchegoyen, C.B., R.J. Alvarez, M.J. Rodriguez, and L. Szczupak. 2011. The activity of leech motoneurons during motor patterns is regulated by intrinsic properties and synaptic inputs. *J Comp Physiol A Neuroethol Sens Neural Behav Physiol*. 198:239-251.

Petersen, P.C., M. Vestergaard, K.H. Jensen, and R.W. Berg. 2014. Premotor spinal network with balanced excitation and inhibition during motor patterns has high resilience to structural division. *Journal of Neuroscience*. 34:2774-2784.

Pouzat, C., O. Mazor, and G. Laurent. 2002. Using noise signature to optimize spike-sorting and to assess neuronal classification quality
. *J Neurosci Methods*. 122:43-57.

Puhl, J.G., and K.A. Mesce. 2008. Dopamine Activates the Motor Pattern for Crawling in the Medicinal Leech. *J. Neurosci.* 28:4192-4200.

Pulver, S. R., Bayley, T. G., Taylor, A. L., Berni, J., Bate, M., and Hedwig, B. (2015). Imaging fictive locomotor patterns in larval *Drosophila*. *J. Neurophysiol*. 114, 2564–2577. doi: 10.1152/jn.00731.2015

Rela, L., and L. Szczupak. 2003. Coactivation of motoneurons regulated by a network combining electrical and chemical synapses. *J. Neurosci.* 23:682-692.

Rela, L., and L. Szczupak. 2007. In situ characterization of a rectifying electrical junction. *J. Neurophysiol.* 97:1405-1412.

Rela, L., S.M. Yang, and L. Szczupak. 2009. Calcium spikes in a leech nonspiking neuron. *J. Comp. Physiol.* 195:139-150.

Rodriguez, M.J., R.J. Alvarez, and L. Szczupak. 2012. Effect of a nonspiking neuron on motor patterns of the leech. *J Neurophysiol*. 107:1917-1924.

Rodriguez, M.J., C.B. Perez-Etchegoyen, and L. Szczupak. 2009. Premotor nonspiking neurons regulate coupling among motoneurons that innervate overlapping muscle fiber populations *J. Comp. Physiol. A*. 195:1432-1351.

Rotstein, H.G., E. Schneider, and L. Szczupak. 2017. Feedback Signal from Motoneurons Influences a Rhythmic Pattern Generator. *J Neurosci*. 37:9149-9159.

Satopaa, V., Albrecht, J., Irwin, D., & Raghavan, B. 2011. Finding a "Kneedle" in a Haystack: Detecting Knee Points in System Behavior. In 2011 31st international conference on distributed computing systems workshops (pp. 166-171). IEEE.

Sengupta, M., and M.W. Bagnall. 2023. Spinal interneurons: diversity and connectivity in motor control. *Annual Review of Neuroscience*. 46:79-99.

Stern-Tomlinson, W., M.P. Nusbaum, L.E. Perez, and W.B. Kristan. 1986. A kinematic study of crawling behavior in the leech, hirudo medicinalis. *J. Comp. Physiol A*. 158:593-603.

Szczupak, L. 2014. Recurrent inhibition in motor systems, a comparative analysis. *J Physiol Paris*. 108:148-154.

Van der Maaten, L., and G. Hinton. 2008. Visualizing data using t-SNE. *Journal of machine learning research*. 9.

Wadepuhl, M. 1989. Depression of excitatory motoneurons by a single neuron in the leech central nervous system. *J Exp Biol.* 143:509-527.

583 Wagenaar, D.A. 2015. A classic model animal in the 21st century: recent lessons from the leech
584 nervous system. *J Exp Biol*. 218:3353-3359.
585 Zhen, M., and A.D. Samuel. 2015. C. elegans locomotion: small circuits, complex functions.
586 *Curr Opin Neurobiol*. 33:117-126.

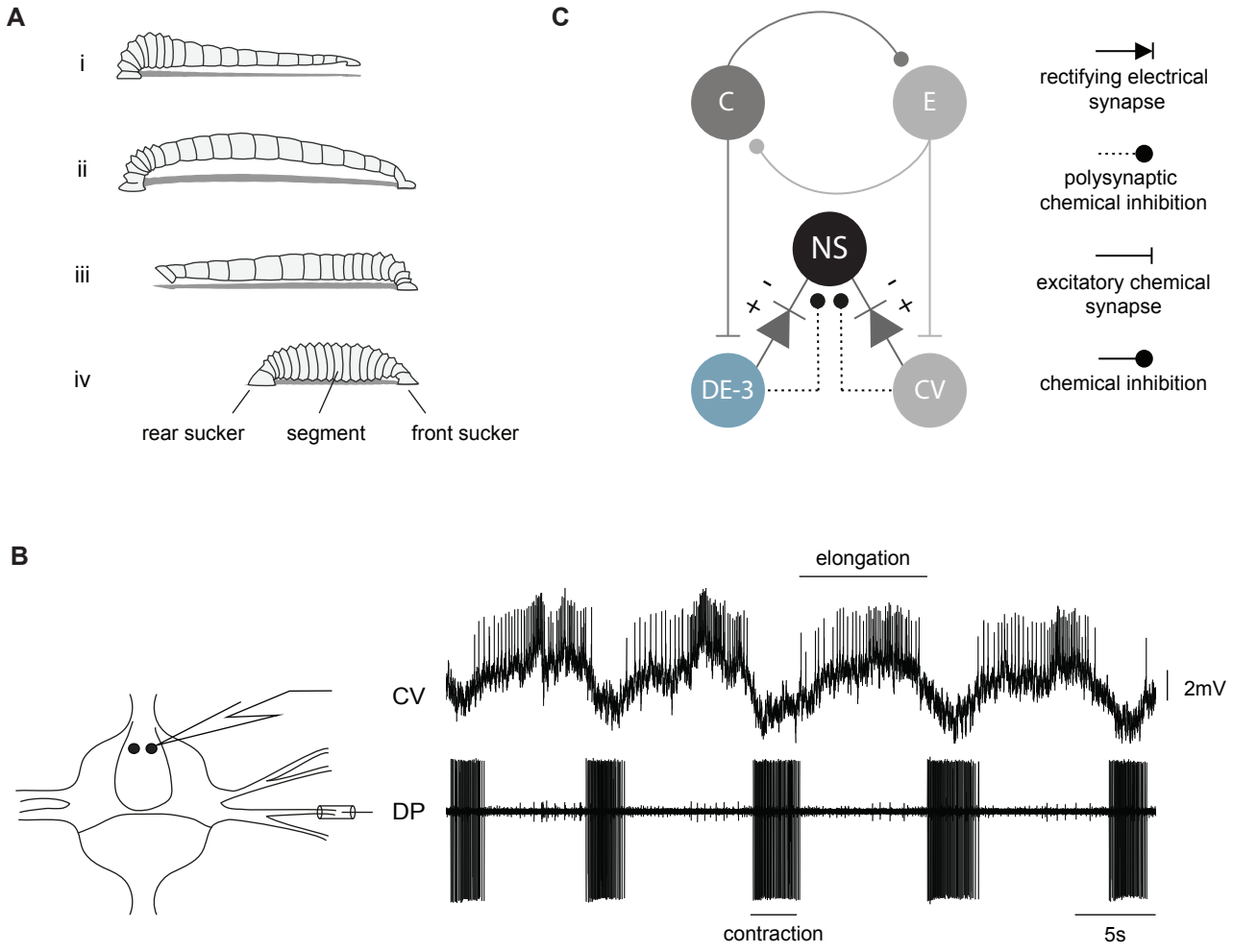

Figure 1. The crawling motor pattern. A. Schematic description of a leech crawling step that results from coordinated waves of elongation (i-ii) and contraction (iii-iv) phases, anchored on front and rear suckers. **B.** Intracellular recording of CV and extracellular recording of DE-3 (in DP nerve) motoneurons during a dopamine-induced crawling episode in an isolated midbody ganglion. Recording diagram on the left. **C.** Putative neuronal circuitry underlying crawling and the recurrent inhibitory circuit in a midbody ganglion. Units C and E correspond to contraction and elongation units of the segmental oscillator, respectively. DE-3 and CV are examples of motoneurons involved in each phase. NS neuron is connected to DE-3 and CV (Rela and Szczupak, 2003; Rodriguez et al., 2009) through chemical and electrical synapses; the + and - symbols indicate the polarity at which the rectifying synapse conducts.

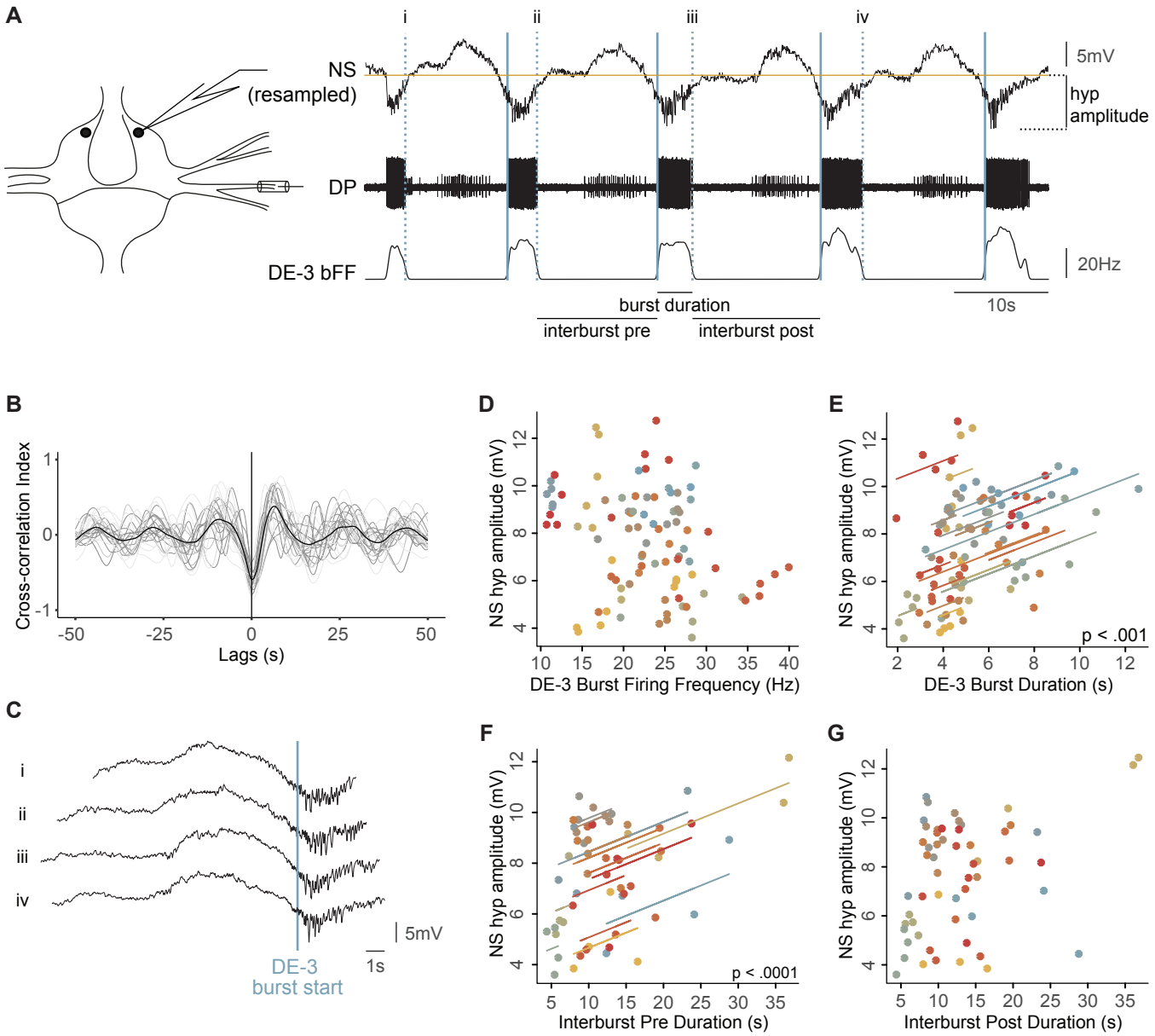

Figure 2. NS activity correlates with the crawling motor pattern. A. NS intracellular recording, DP extracellular recording and DE-3 binned firing frequency (bFF) during a crawling episode. NS recording was resampled to match the data rate of DE-3 bFF. Recording diagram on the left. The blue vertical line marks the beginning and the blue dotted line the end of each DE-3 burst. Different crawling features and NS hyperpolarization amplitude (NS hyp amplitude) are indicated. **B.** Cross-correlograms of the DE-3 bFF curves and NS resampled traces. Each gray trace corresponds to an individual experiment. The black curve corresponds to the mean cross-correlogram. (n = 23 crawling episodes containing 5 cycles, obtained in 23 ganglia from 18 leeches). **C.** Successive cycles of the NS recording shown in panel A, segmented at the times indicated by the dotted lines and aligned by the times indicated by solid blue lines indicated in A. **D.** NS hyperpolarization amplitude as a function of DE-3 Burst FF. **E.** Like in D, as a function of DE-3 burst duration. **F.** Like in D, as a function of interburst lag preceding DE-3 bursts. **G.** Like in D, as a function of the interburst lag after DE-3 bursts. For D-G, n = 19 crawling episodes, with 5 cycles each. In D to G, the correlation was tested using linear mixed-effects models, contemplating different experiments as a random variable. In D and G, $p>0.05$, and in E and F, $p<0.05$. The lines correspond to regressions obtained from the linear mixed-effects model. The coefficients were 0.374 ± 0.089 mv/s for E and 0.122 ± 0.034 mv/s for F.

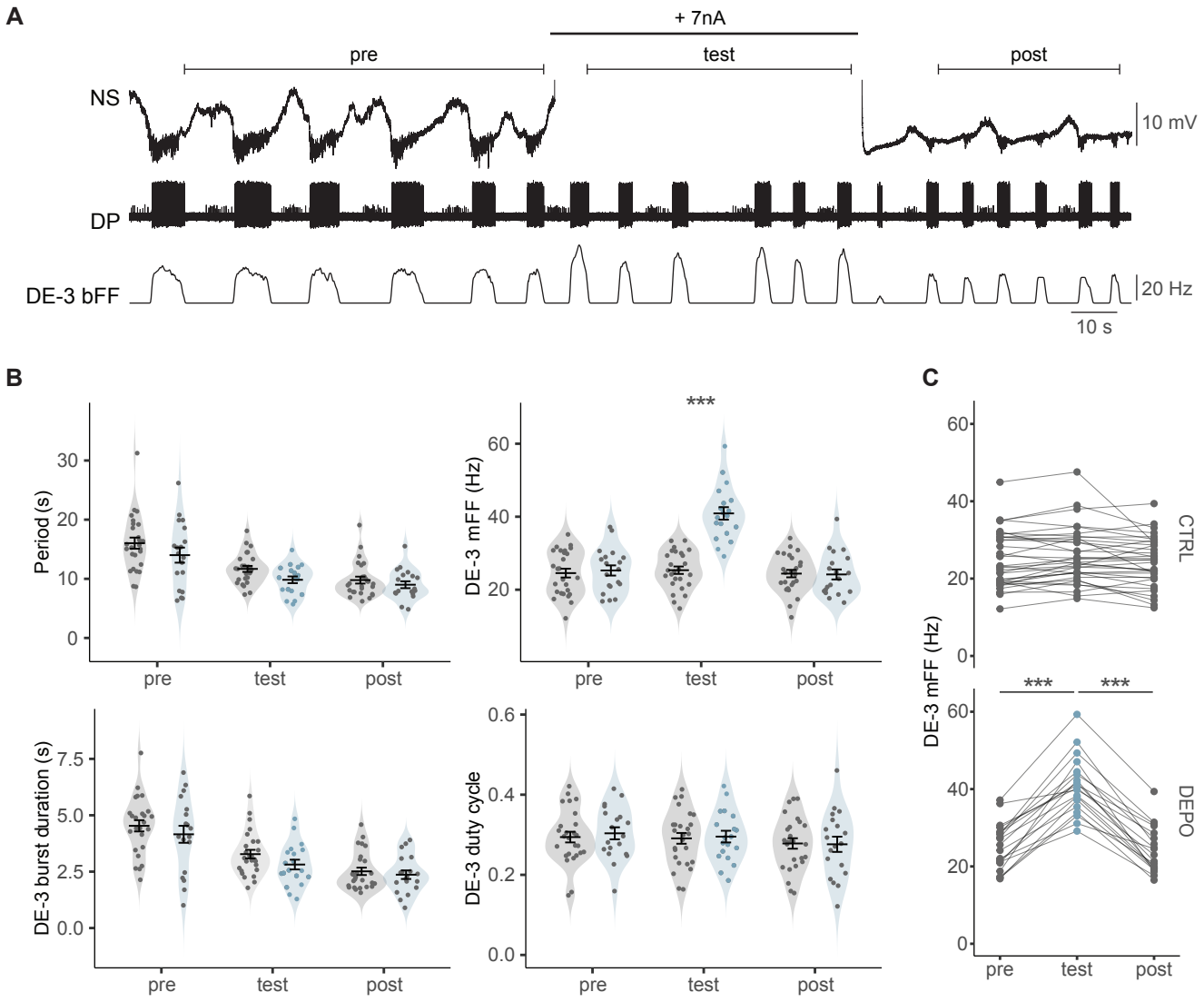

Figure 3. Effect of NS on crawling. A. Intracellular NS and extracellular DP recordings during a dopamine-induced crawling episode. A +7 nA pulse was injected in NS at the time indicated by the thick line. Segments above the recordings mark three epochs: previous (pre), during (test) and after (post) the pulse. **B.** Crawling period (end-to-end), DE-3 mFF, burst duration and duty cycle for cycles in the three epochs marked in A, for control experiments where no current was injected in NS (gray violins, n= 120 cycles from 26 episodes in 26 ganglia from 16 leeches) and for experiments where NS was depolarized (light blue violins, n= 92 cycles from 19 episodes in 19 ganglia from 15 leeches); each point corresponds to the mean value during the epoch for each individual experiment. Bars provide the mean ± SEM. *** $p<0.001$ (interaction between epoch and treatment factors). **C.** Mean DE-3 mFF for the three epochs from each individual experiment for control (CTRL) and depolarizing (DEPO) tests. Lines link dots that correspond to each individual experiment. *** $p<0.001$ (pairwise simple contrasts, Δ pre-test = -15.591 ± 1.037 Hz and Δ test-post = 16.648 ± 0.919 Hz).

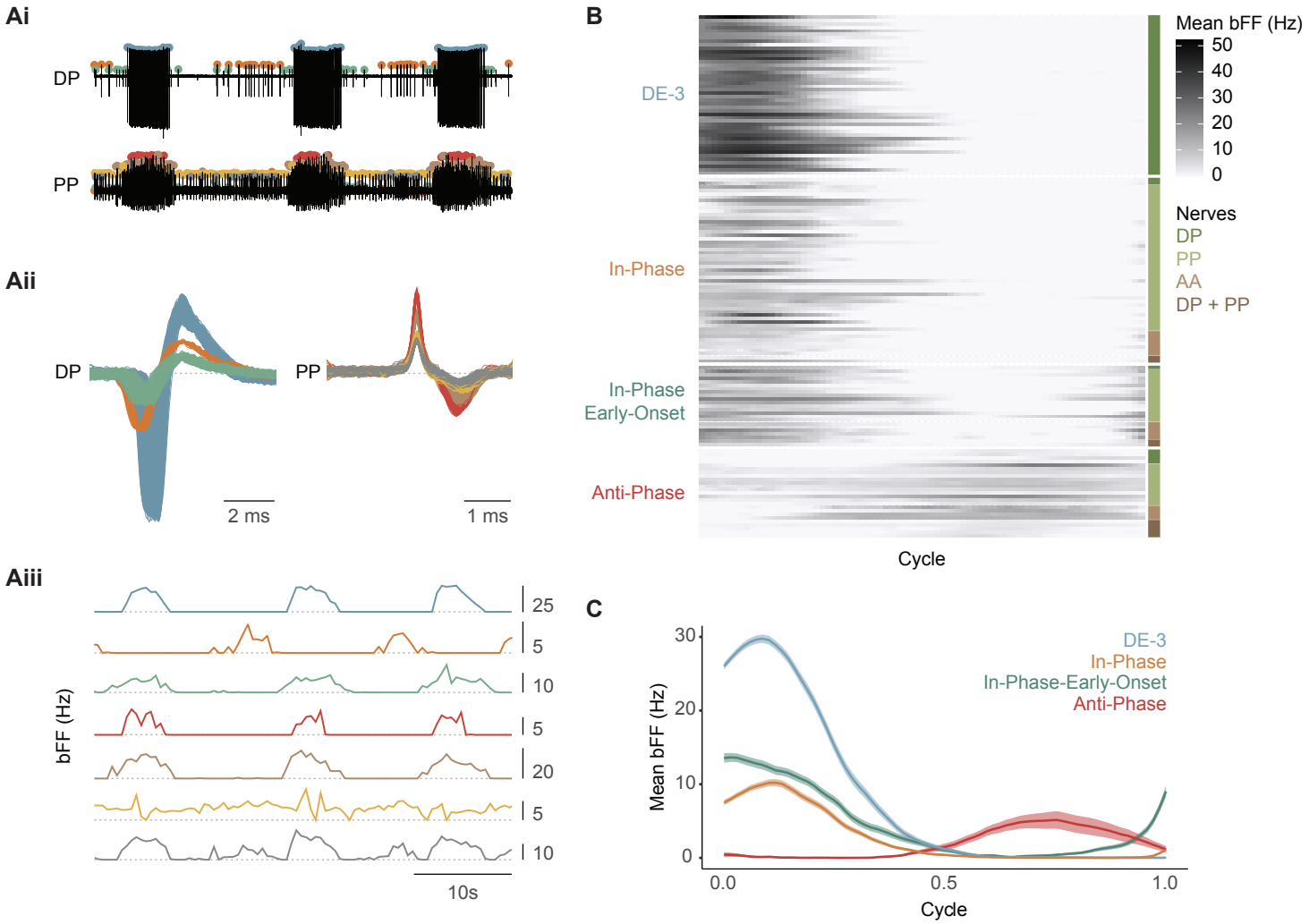

Figure 4. Profile of motoneuron activity during crawling. A.i. Representative example of a spike sorting analysis implemented in paired extracellular recordings of DP and PP nerves during a crawling episode. Each color dot singles out a distinct active unit along the recordings. **A.ii.** Spikes waveforms corresponding to spikes detected in the DP and PP nerves in Ai. **A.iii.** bFF calculated for each unit identified in A. The horizontal dotted lines indicate bFF = 0 Hz. Scales on the right are in Hz. **B.** Raster plot showing mean bFF along a cycle, set from the first spike of a DE-3 burst to the first spike in the next burst, obtained from 147 rhythmic units identified in DP, PP and AA nerves (n = 46 ganglia in 24 animals). The values are the mean of 4 crawling cycles for each unit. The units were classified into four groups, indicated on the left. The nerves from which the motoneuron activity was recorded are indicated on the right. The gray scale on the right indicates the bFF value in Hz. **C.** Mean bFF for all the units included in each group. The shaded area represents the standard error of the mean.

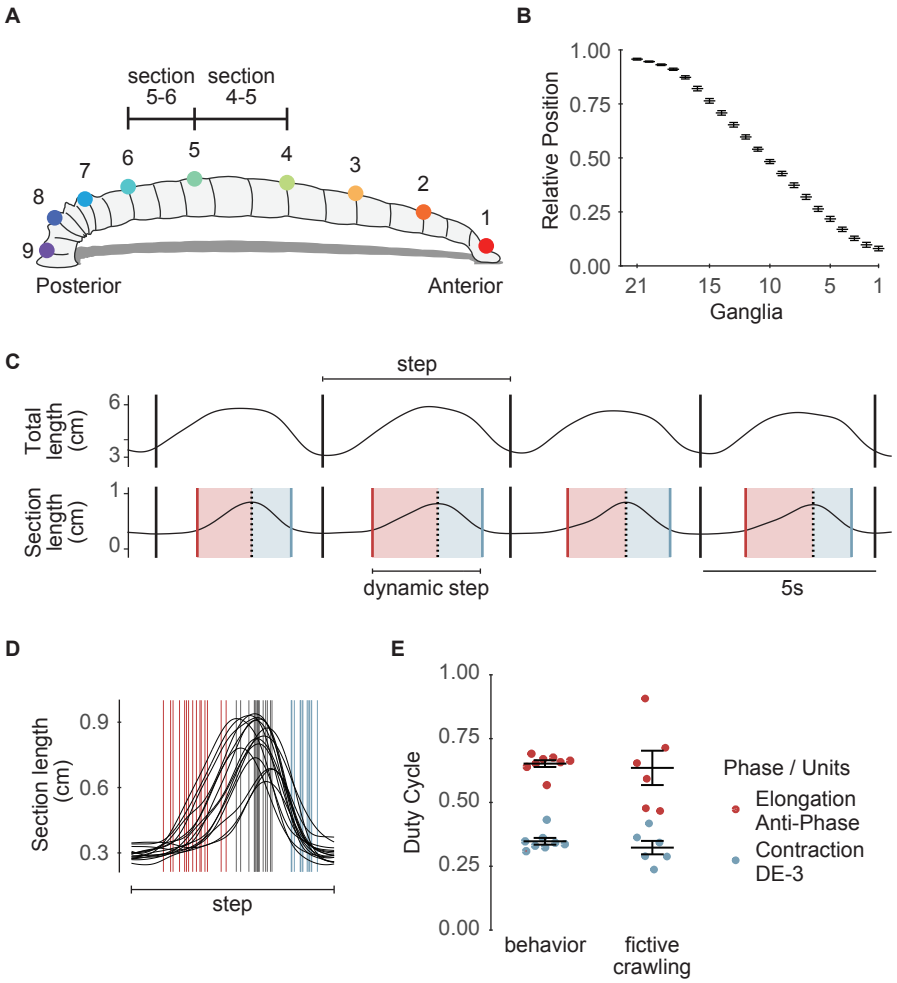

Figure 5. Analysis of leech crawling. A. Schematic representation of a leech with nine points as painted on their dorsal midline. The sections between points 4-5 and 5-6 comprise ganglia 8-15 that were used for the electrophysiological analysis. **B.** Relative position of midbody ganglia 1–21. Mean and standard error of the mean are shown (n = 3) (Kearney et al. 2022). **C.** Representative example of the changes in total length and section 4-5 of a leech during four steps as the animal was crawling. The limits of each step are indicated by black vertical lines (see Materials and Methods); red and blue vertical lines mark the start of elongation and the end of contraction, respectively; black dashed vertical lines indicate the maximal section length. Light red and blue shades indicate elongation and contraction phases, respectively. **D.** Superimposed length curves of a section across random multiple steps (n= 15 of 76 total steps for this animal) of one leech. **E.** Duty Cycle of the elongation and contraction phases measured in crawling behavior or in fictive crawling. Behavioral variables were calculated as the duration of each phase relative to the sum of elongation and contraction phases (dynamic step in C), excluding isometric phases. Points represent the mean for each leech, while bars and lines indicate the mean ± SEM across all leeches (n = 249 steps from 8 leeches). For the Duty Cycle of DE-3 and Anti-Phase units, points correspond to the mean for each ganglion, with bars and lines showing the mean ± SEM across all ganglia (n = 4 cycles for each DE-3 or Anti-Phase motoneuron, 6 ganglia, 6 leeches).

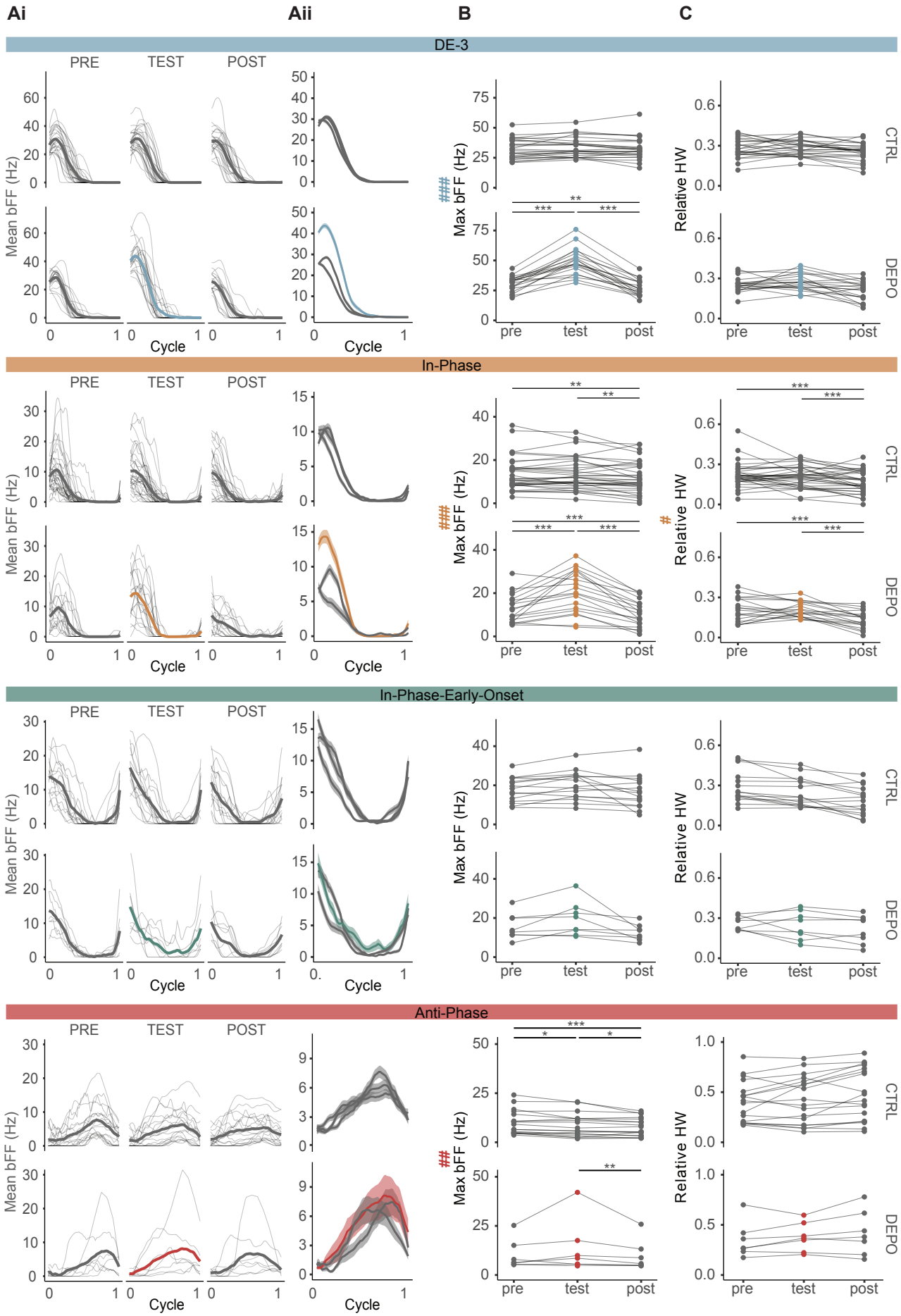
Ai
Aii
B
C
DE-3
In-Phase
In-Phase-Early-Onset
Anti-Phase
PRE
TEST
POST
Mean bFF (Hz)
Cycle
Max bFF (Hz)
Relative HW
CTRL
DEPO
pre
test
post
###
#
##
**
***
*

Figure 6. Effect of NS on the different phases of crawling. A.i. Mean bFF along cycles in pre, test, and post epochs for each unit within the four groups described in Figure 4. For each unit type the upper line of graphs presents control experiments, where no current was injected in NS, and the bottom line, depolarization experiments, where 5-7 nA current steps were injected in NS during the test epoch. Thin lines show the mean bFF (including 4 - 6 cycles) for each experiment, and thick lines show the overall mean. **A.ii.** Superimposition of the overall bFF mean of the three epochs. The shaded area presents the standard error of the mean. **B** & **C.** Maximum bFF (Max bFF) and Relative Half Width (Relative HW) measured in each individual unit. A-C are plotted for each of the four groups of units indicated. Lines connect the mean values across each epoch within the same experiment. Mixed-effects models with two fixed factors were performed; on the left of the B and C panel, # indicates a significant interaction between treatment and epoch factors; * indicates significant differences for pairwise simple contrasts between epochs, within each treatment. *, ** and *** (or #) indicate $p<0.05$, $p<0.01$ and $p<0.001$, respectively. Supplementary Table 2 describes the statistical models performed. For DE-3, n= 26 control and 20 depolarization ganglia, from 46 ganglia; for In-Phase, n= 38 units for control and 21 units for depolarization, from 30 ganglia; for Anti-Phase, n= 18 units for control and 7 units for depolarization experiments, from 22 ganglia; and for In-Phase-Early-Onset, n= 15 units for control and 8 units for depolarization experiments, from 23 ganglia.

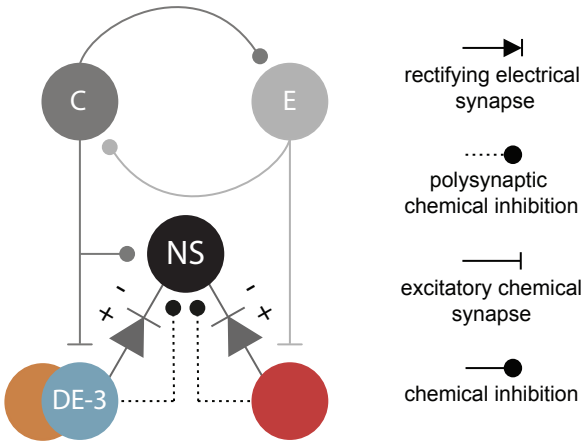

Figure 7. NS in the crawling circuitry. Putative neuronal circuitry as described in Figure 1C, including the connection between the oscillatory circuit and NS.

Effect of NS depolarization on *crawling* features. (n units = 26 ctrl, 19 depo / n leeches = 16 ctrl, 15 depo).					
Variable	Model, random effects	Significance of factor interactions	Pairwise simple contrasts		
			Comparison	Ratio	p value
DE-3 FF	LMM intercept - unit slope - epoch	<.0001	ctrl depo / pre post / pre post / depo depo depo / pre post / pre post / depo	 1.04 1 0.96 1.62 0.96 0.59	 0.6345 0.9815 0.4654 <.0001 0.3909 <.0001
DE-3 burst duration	GLMM - Gamma family, log link intercept - unit slope - epoch	0.3077	-	-	-
period	GLMM - Gamma family, log link intercept - units	0.2107	-	-	-
DE-3 duty cycle	LMM intercept - unit slope - epoch	0.8309	-	-	-
Effect of temporal drift on *crawling* features. (n units = 26 ctrl, 19 depo / n leeches = 16 ctrl, 15 depo)					
Variable	Model, random effects	Significance of factor	Fixed effects		
			Epoch	Estimate	p value
DE-3 burst duration	GLMM - Gamma family, log link intercept - unit	<.0001	pre (intercept) depo post	4.40 3.16 2.44	<.0001 <.0001 <.0001
period	GLMM - Gamma family, log link intercept - unit	<.0001	pre (intercept) depo post	15.45 11.45 9.47	<.0001 <.0001 <.0001
DE-3 duty cycle	LMM intercept - unit	0.1623	-	-	-

Supplementary Table 1. Statistical Models Performed for the Effect Analysis of NS depolarization on *crawling* features and DE-3 activity during the fictive behavior.

Variable	Model, random effects	Significance of factor interactions	Pairwise simple contrasts		
			Comparison	Ratio	p value
Effect of NS depolarization on motoneuron activity during *crawling*.					
DE-3 (n units = 26 ctrl, 20 depo / n cycles = 110 ctrl, 99 depo / n leeches = 16 ctrl, 16 depo)					
Max FF	LMM intercept - unit slope - treatment and epoch	<.0001	ctrl depo / pre post / pre post / depo depo depo / pre post / pre post / depo	 1.04 1 0.96 1.59 0.89 0.56	 0.5512 0.9995 0.5406 <.0001 0.0066 <.0001
Rel HW	LMM intercept - unit slope - treatment and epoch	0.1596	-	-	-
In-Phase (n units = 34 ctrl, 19 depo / n cycles = 149 ctrl, 93 depo / n experiments = 17 ctrl, 11 depo / n leeches = 13 ctrl, 8 depo)					
Max FF	GLMM - t_family, identity link intercept - experiment/unit	<.0001	ctrl depo / pre post / pre post / depo depo depo / pre post / pre post / depo	 1.01 0.92 0.91 1.52 0.86 0.56	 0.9628 0.0046 0.0014 <.0001 0.0005 <.0001
Rel HW	GLMM - t_family, identity link intercept - experiment/unit	0.01492	ctrl depo / pre post / pre post / depo depo depo / pre post / pre post / depo	 0.93 0.78 0.84 0.99 0.60 0.61	 0.1788 <.0001 0.0007 0.9840 <.0001 <.0001
Anti-Phase (n units = 18 ctrl, 7 depo / n cycles = 78 ctrl, 34 depo / n experiments = 15 ctrl, 7 depo / n leeches = 12 ctrl, 7 depo)					
Max FF	GLMM - t_family, identity link intercept - experiment/unit	0.00148	ctrl depo / pre post / pre post / depo depo depo / pre post / pre post / depo	 0.91 0.82 0.90 1.10 0.94 0.85	 0.0104 <.0001 0.0180 0.0505 0.4132 0.0025
Rel HW	GLMM - t_family, identity link intercept - experiment/unit	0.9791	-	-	-
In-Phase-Early-Onset (n units = 15 ctrl, 8 depo / n cycles = 66 ctrl, 45 depo / n experiments = 12 ctrl, 5 depo / n leeches = 11 ctrl, 5 depo)					
Max FF	LMM intercept - experiment/unit	0.0891	-	-	-
Rel HW	GLMM - t_family, identity link intercept - experiment/unit	0.173	-	-	-

Supplementary Table 2. Statistical Models Performed for the Effect Analysis of NS depolarization on different groups of units activity during *crawling*.